ELECTROCHEMISTRY

An ion redistributor for dendrite-free lithium metal anodes

Chen-Zi Zhao, Peng-Yu Chen, Rui Zhang, Xiang Chen, Bo-Quan Li, Xue-Qiang Zhang, Xin-Bing Cheng*, Qiang Zhang*

Lithium (Li) metal anodes have attracted considerable interest due to their ultrahigh theoretical gravimetric capacity and very low redox potential. However, the issues of nonuniform lithium deposits (dendritic Li) during cycling are hindering the practical applications of Li metal batteries. Herein, we propose a concept of ion redistributors to eliminate dendrites by redistributing Li ions with Al-doped $Li_{6.75}La_3Zr_{1.75}Ta_{0.25}O_{12}$ (LLZTO) coated polypropylene (PP) separators. The LLZTO with three-dimensional ion channels can act as a redistributor to regulate the movement of Li ions, delivering a uniform Li ion distribution for dendrite-free Li deposition. The standard deviation of ion concentration beneath the LLZTO composite separator is 13 times less than that beneath the routine PP separator. A Coulombic efficiency larger than 98% over 450 cycles is achieved in a Li | Cu cell with the LLZTO-coated separator. This approach enables a high specific capacity of 140 mAh g^{-1} for $LiFePO_4$ | Li pouch cells and prolonged cycle life span of 800 hours for Li | Li pouch cells, respectively. This strategy is facile and efficient in regulating Li-ion deposition by separator modifications and is a universal method to protect alkali metal anodes in rechargeable batteries.

INTRODUCTION

Lithium (Li) metal anodes are strongly considered one of the most promising candidates for next-generation high-energy density rechargeable batteries due to their extremely high theoretical specific capacity of 3860 mAh g^{-1} and low reduction potential (−3.04 V versus standard hydrogen electrode) (*1*). However, rechargeable Li metal batteries are suffering from limited cycle life, low cycling efficiency, and severe safety concerns resulting from sharp Li dendrites and electrolyte degradation (*2*–*4*). Research to solve these challenging issues originated decades ago and has had a renaissance recently due to the rapid developments of Li-sulfur and Li-oxygen batteries with high theoretical energy densities (*5*).

The uncontrollable growth of Li dendrites is an extremely complicated issue coupled with the transport of Li ions and electrons, as well as the chemical and electrochemical reactions at the anode-electrolyte interphase (*6*). Tremendous efforts have been devoted to handling this challenging issue. Conductive Li hosts, such as graphene (*7*), nitrogen-doped graphene, and three-dimensional (3D) porous copper (*8*), are designed to regulate the deposition of Li ions to deliver a uniform and stable metallic anode. The large specific surface area of these conductive frameworks lowers the local current density, which effectively extends the Sand's time and improves cell safety. Also, the ion distribution in the electrolyte can be effectively controlled by the matrix size, pore structure, and surface functional groups of these frameworks. Simultaneously, electrolyte additives (*9*, *10*), porous separators (*11*), artificial protective films (*12*), and solid-state electrolytes (*13*–*17*) are applied to govern Li-ion diffusion and control electrochemical reactions to achieve a homogeneous Li deposition. These methods afford fresh insights into Li metal anode protection and achieve stable cycling performances. However, there are dendritic issues in practical cells with large capacities at high current densities (*18*). A mechanistic understanding of the dendritic growth is still lacking. If the transport behavior of Li ions and electrons can be rationally decoupled, a safe and long–life span Li metal battery is therefore highly expected (*19*, *20*).

Beijing Key Laboratory of Green Chemical Reaction Engineering and Technology, Department of Chemical Engineering, Tsinghua University, Beijing 100084, China. *Corresponding author. Email: cxb12@mails.tsinghua.edu.cn (X.-B.C.); zhang-qiang@mails.tsinghua.edu.cn (Q.Z.)

The migration of Li ions in an electrolyte and solid electrolyte interphase (SEI), which is usually the rate-determining step of Li-ion deposition, is much slower than the transport of electrons in conductive matrices (*21*–*23*). Li ions migrate between cathodes and anodes through electrolytes and separators repeatedly to experience the electrochemical reactions in rechargeable batteries (*24*, *25*). Because of the ionically insulated nature of the commercial separator skeleton, the electrolytes in the separators pave the way for Li-ion transport between cathodes and anodes. Since electrolytes are mostly trapped in separator pores, Li ions are very crowded near the pores after crossing the separators. This leads to the enrichment of Li ions on the anode surface facing the pores of the separators while there is a lack of Li ions on the anode surface facing the skeletons of the separators. The anisotropic distribution of Li ions on the anode surface result in the heterogeneous nucleation and deposition of Li ions and lastly dendritic Li growth and rapid cell life-span termination. Lithiophilic modifications to improve the ionic conductivity and modulus strengthening to stop dendrite permeation are conducted on the separators (*26*–*28*). However, these methods still cannot handle the dilemma of the anisotropic distributions of Li ions induced by the ionically insulated nature of the separator skeleton. Therefore, regulating the Li-ion diffusion through the separator is a primary solution to suppress Li dendrite growth and prolong the battery life span.

In this contribution, we propose a concept of ion redistributors to homogenize Li ions after they cross the separators, prepared by coating commercial polypropylene (PP) separators with solid-state fast ionic conductors [Al-doped $Li_{6.75}La_3Zr_{1.75}Ta_{0.25}O_{12}$ (LLZTO)]. Ion migration in batteries can be analogized to the fluid transportation in packed towers in the field of chemical industry. Redistributors are used to intensify the heat and mass transfer processes in a packed tower. The LLZTO coating layer can act as a redistributor to regulate Li-ion distribution because of its abundant 3D ion conduction channels (Fig. 1). Compared with routine PP separators where ions congest near the pores, the LLZTO layer with abundant 3D ion conduction channels can disperse the concentrated Li ions in liquid electrolytes to realize a uniform distribution. Instead of stopping Li dendrites from permeating the separators by stiff coating with high mechanical modulus, this strategy can guide Li ions to a uniform distribution and transform the Li dendrites to a dense and smooth Li deposition. This method contributes to constructing a dendrite-free Li metal anode with limited liquid electrolytes, rendering a prolonged life span in both coin and

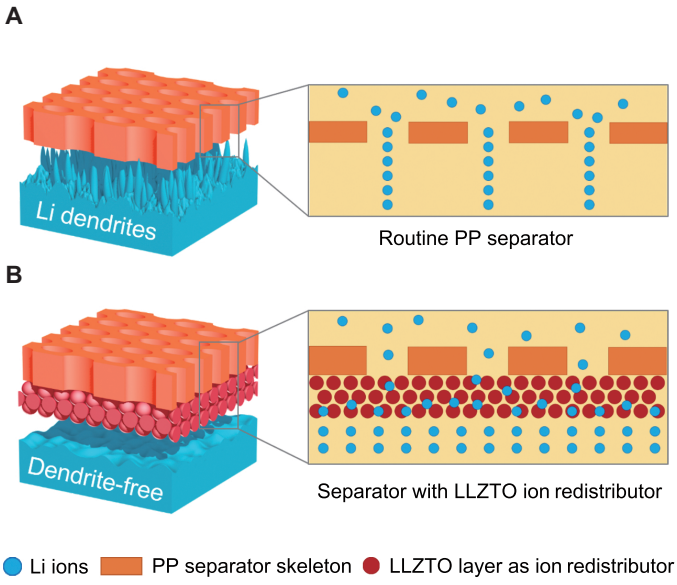

Fig. 1. Schematic illustration of the electrochemical deposition behaviors of the Li metal anodes using (**A**) a routine PP separator and (**B**) a composite separator with the LLZTO layer as an ion redistributor to uniform Li-ion distribution.

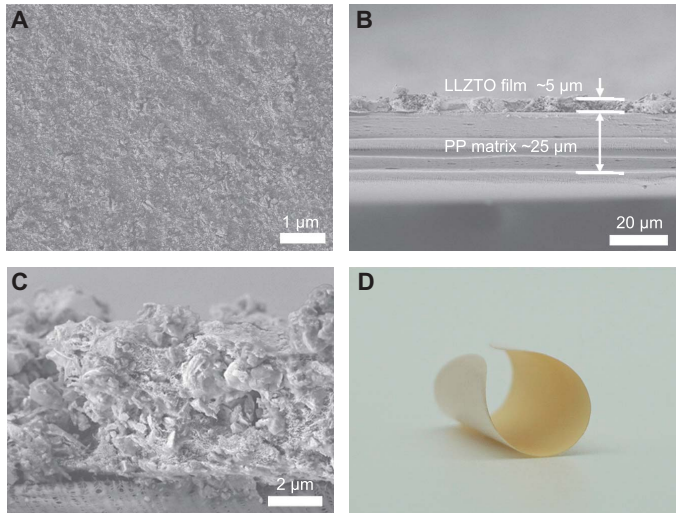

Fig. 2. Morphological characterizations of the composite separator with the LLZTO layer as an ion redistributor. (**A**) Scanning electron microscope (SEM) and digital images of the surface of composite separators. (**B** and **C**) Cross section of the composite separator exhibiting (B) an overall view consisting of the LLZTO film and the PP matrix and (C) the LLZTO layer. (**D**) Digital image of the composite separator at a bending state.

pouch cells. In addition, the LLZTO coating strategy is quite facile to realize and convenient to match the current cell industry without great changes in electrolytes and electrode processing. Therefore, the concept of separator modification by LLZTO redistributors is expected to achieve a dendrite-free Li deposition in practical batteries.

RESULTS

Structure and morphology

Al-doped LLZTO is one of the most promising solid-state electrolytes due to its high ionic conductivity, excellent chemical stability, super mechanical strength, and desirable electrical insulation (*29*). LLZTO powders are well dispersed by sonication in tetrahydrofuran (THF) solvent and coated on one side of the commercial PP separator (Celgard 2400) by vacuum filtration. The adopted LLZTO powders exhibit a cubic garnet phase (PDF 80-0457) (fig. S1), whose ionic conductivities are much higher than those of its tetragonal counterparts (*30*). The dark-field transmission electron microscope (TEM) image indicates that the crystal size of the ceramic particles is around 20 nm (fig. S2). X-ray diffraction (XRD) patterns of the composite electrolytes reveal that the LLZTO layer is integrated to a PP matrix without losing its garnet crystalline structure.

As indicated in fig. S3, many large pores are observed on the bare PP separator. These pores are fully and uniformly covered by LLZTO particles (Fig. 2A). A thin layer of the ceramic coating with a typical thickness of 5 μm and the mass loading of around 0.9 mg cm^{-2} is well attached to the PP matrix without delamination (Fig. 2, B and C). Because of its thin feature, the prepared composite separators can be fully bended and exhibit great potential for practical applications in flexible Li batteries (Fig. 2D). The composite separator is also stable at elevated temperature, strengthening the battery safety (fig. S4).

Ion transport

The routine PP separator is not ionically conductive. Its conductivity is contributed by the packed electrolytes in its pores. The distribution of ions through the routine PP separator is modeled in Fig. 3A, where Li ions move through the separator in the *y* direction (fig. S5). Ions are concentrated in the neighboring pores of the commercial PP separator due to the inert Li-ion conductivity of the PP separator (*31*). The pores in PP filled with liquid electrolytes are the only pathway for Li-ion migration. Hence, Li ions are centered in the holes filled with liquid electrolytes during deposition, resulting in an extremely nonuniform ion distribution of Li^+ flux after the PP separator (fig. S6, cyan line). Furthermore, turbulences of ion distributions, which are probably caused by partial electrode material failure or local electric field change, are difficult to avoid completely in practical working batteries. The routine separators are incapable of inhibiting those irregularities, resulting in a severe nonuniform Li deposition.

In contrast, Li ions can be uniformly redistributed by the abundant 3D Li transportation channels of the LLZTO layer (Fig. 3B) in LLZTO composite separators, contributing to a homogeneous Li distribution. The Li-ion concentrations along the routine PP (cyan line) and composite separator surface (orange line) are compared in fig. S6 and table S1. Large ion concentration fluctuations exhibit inhomogeneous ion distribution in a routine PP separator, where the standard deviation (SD) of ion concentration beneath the PP separator is 13 times higher than that beneath the LLZTO composite separator (table S1). In the LLZTO layer, Li ions migrate in the *y* direction, but the transverse diffusion is also enhanced because of the rich 3D Li-ion migration pathways in the garnet LLZTO with favorable inter- and intragrain conductivities (*32*). It has been revealed that the Ta doping does not alter the topology of ion transportation channels in $Li_7La_3Zr_2O_{12}$ (LLZO) conductors (*33*), where the abundant 3D ion migration pathways have been indicated by various researchers (*34*, *35*).

The abundant 3D ion transport channels in the garnet ceramic layers can be ascribed to pathways within the crystal structure, along the grain boundaries, and through the particle interfaces. First, the cubic garnet Al-doped LLZTO ceramics in the composite separator are synthesized with excess Li atoms occupying the octahedral sites,

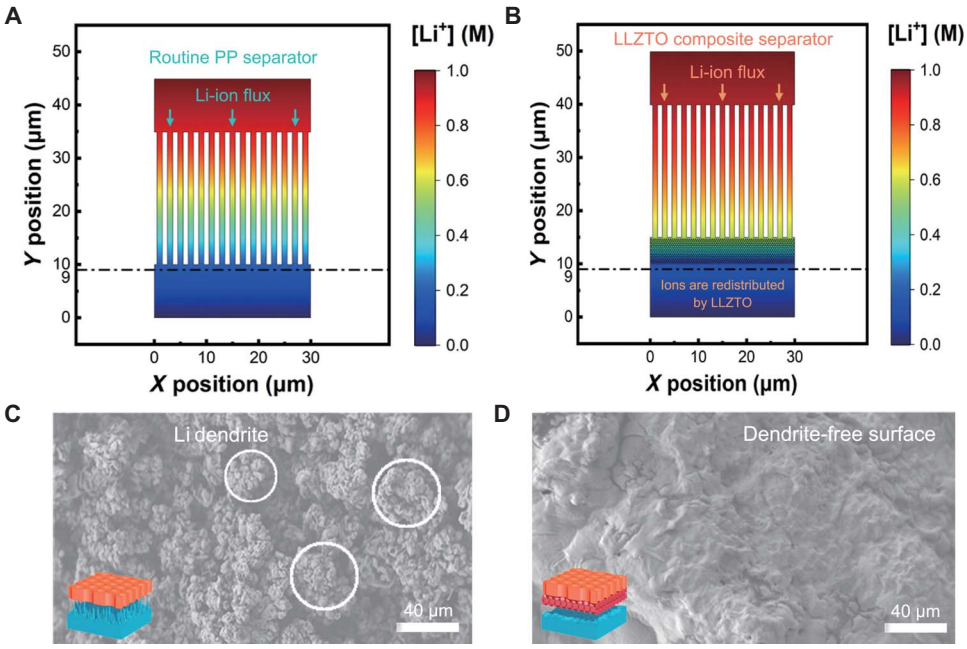

Fig. 3. Ion transportation behaviors in a routine PP separator and the composite separator with the LLZTO layer as an ion redistributor. (**A**) Distributions of Li ions through routine PP separator and (**B**) LLZTO composite separator. Colors in the graph represent the concentration of Li ions ([Li^+]). (**C** and **D**) SEM images of Li metal deposits through (C) routine PP separator and (D) composite separator.

which can be migrated through static repulsion and dynamic processes along the path of one octahedral site, one tetrahedral site, and one vacant octahedral site (*36*). In a cubic structure, the increase in the equivalent Li-ion positions owing to the high symmetry leads to increased Li vacancies. Furthermore, there are plenty of highly disordered octahedral and tetrahedral sites, indicating fast Li-ion transport channels in multiple directions (*37*). Second, the conductivities along the grains in a garnet-type structure are regarded as nearly the same order of magnitude compared with those within the crystal structures, realizing multidirectional ion migration channels in polycrystalline LLZTO (*38*). Third, the ion transport phenomenon has been observed through interfaces between ceramic particles and polymer phase. Although ion transportation through particle interfaces is not as efficient compared with LLZTO particles with outstanding ionic conduction ability (*39*), the transit capability will be greatly enhanced when small amounts of liquid electrolytes are added in the system.

SEM analyses were further carried out to demonstrate the effects of the LLZTO ion redistributor on Li metal deposition at a current density of 0.5 mA cm^{-2} under composite separators, with a LLZTO layer facing Li metal. An electrolytic cell (fig. S7) and a coin cell with a polytetrafluoretyhylene (PTFE) circle (fig. S8) were used to avoid the effect of additional stress on Li depositing behavior. Quantities of sharp Li dendrites are observed with a routine PP separator (Fig. 3C and fig. S9B). The bushy Li dendrites indicate a large surface area of Li deposits, causing more contact between the Li metal anode and liquid electrolytes, and a rapid consumption of the electrolytes, which can seriously accelerate failure of a rechargeable battery. In comparison, the surface of Li deposits in Fig. 3D and fig. S9A exhibits a dense layer containing flat, rounded, and uniform Li metal hills beneath the composite separator. Therefore, the LLZTO-coated separators redistribute and spread the ions to a much more homogeneous distribution during electrochemical reactions, bringing about a dendrite-free morphology.

Long-term electrochemical cycles

The applications of the composite separators with a LLZTO layer for Li metal anodes were investigated by Li | Cu half cells, Li | Li symmetrical cells, and Li | $LiFePO_4$ (LFP) full cells. Coulombic efficiency (CE) measures the amount of irreversible Li metal consumptions during repeated cycles due to the formations of SEI films and dead Li, which will directly affect the cycle life of a practical battery (*40*). During cycling, a fixed amount of Li ions migrates through the separator and plates on a Cu substrate, and then the deposited Li is stripped away. Coulombic efficiency is defined as the ratio of Li that is stripped from the working electrode versus the plated Li metal.

Batteries with a LLZTO composite separator exhibit a more stable cycling, with enhanced Coulombic efficiency and a longer cycle life in both ether-based 1,3-dioxolane (DOL)/1,2-dimethoxyethane (DME) electrolytes and carbonate-based ethylene carbonate (EC)/diethyl carbonate (DEC) electrolytes than those with routine PP separators. The cells render high efficiency above 98% over 450 cycles in ether-based electrolytes (Fig. 4A and fig. S10). The initial low Coulombic efficiency is ascribed to the activation reactions between LLZTO or ether-based liquid electrolytes and Li metal, forming an interconnected solid-state Li conduction layer on the Li metal anodes. In comparison, batteries with routine PP separators present a sharp efficiency decay after 200 cycles. Although the Coulombic efficiency of a PP separator is as high as that of a composite separator in the first 200 cycles, it declined rapidly after 200 cycles, indicating that the Li metal loss resulted from electrolyte depletion and nonuniform Li deposition. The charge and discharge curves at the 300th and 400th cycles also exhibit the enhancement in electrochemical deposition (fig. S10). The cells with the LLZTO composite separator render stable cycling with high efficiency, while there are obvious fluctuations during discharging on both the 300th and 400th cycles in the routine PP separator due to the unstable Li migration states.

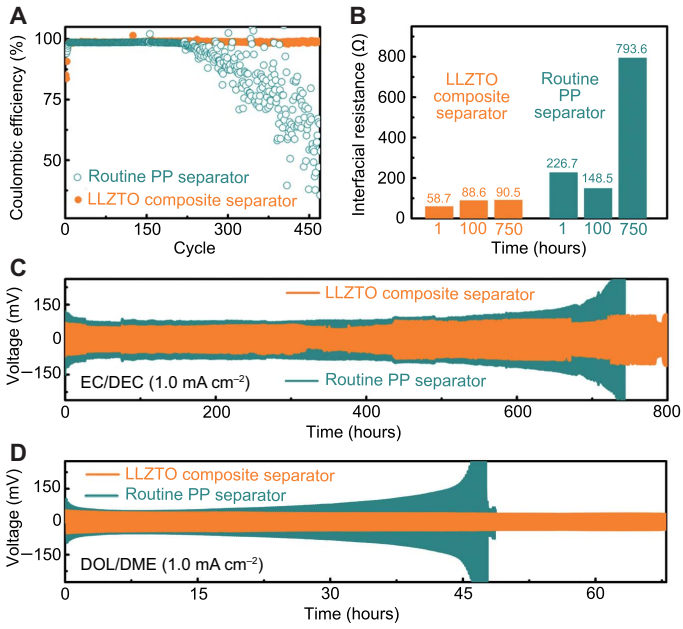

Fig. 4. Electrochemical performances of cells using composite separators with the LLZTO layer as an ion redistributor and routine PP separator. (**A**) Variations of Coulombic efficiency with cycle numbers in Li I Cu cells at a current density of 0.5 mA cm^{-2} in ether-based (DOL/DME) electrolytes. (**B**) Interfacial resistance in Li-Li cells calculated from impedance spectra after 1-, 100-, and 750-hour cycling. (**C** and **D**) Voltage profiles for Li I Li symmetric cells using (C) carbonate-based EC/DEC electrolytes and (D) ether-based DOL/DME electrolytes at a current density of 1.0 mA cm^{-2}.

The long-term interfacial stabilities were further investigated through symmetrical Li metal | separator | Li metal cells based on ether- and carbonate-based electrolytes. During cycling, Li ions are transported back and forth between the two Li metal electrodes at a high current density of 1.0 mA cm^{-2}. The voltage versus time plot is depicted in Fig. 4 (C and D). For a EC/DEC electrolyte system, the voltage hysteresis of Li | Li cells with routine PP separators (cyan line) is as large as 0.18 V, then diverges and goes beyond 0.30 V after 700-hour cycling, indicating that the electrolyte is nearly depleted resulting from the gradually accumulated Li dendrites and dead Li. In comparison, the cells with a LLZTO composite separator render a constant and stable voltage profile (80 mV) for 800 hours, suggesting a uniform Li metal electrode with a stable interface. A similar behavior can be observed in a DOL/DME electrolyte system (Fig. 4D). Compared with batteries with routine PP separators, the batteries with LLZTO layers render a tighter voltage hysteresis (73 mV versus >200 mV for the routine PP separator) and much more extended cycle life (75 hours versus <50 hours for the routine PP separator), indicating that the dendrites are controlled effectively.

The cycling performance is also enhanced under a current density of 0.5 mA cm^{-2} in both carbonate-based (fig. S11) and ether-based (fig. S12) electrolytes, where the interfacial stability is greatly improved in 800-hour cycling by using LLZTO layers. All cells with LLZTO layers exhibit enhanced performances, owing to the well-distributed Li ions and dendrite-free Li metal electrodes.

The electrochemical impedances of Li | Li symmetrical cells in EC/DEC electrolytes at 1.0 mA cm^{-2} were measured at the end of 1-, 100-, and 750-hour cycling. The results were analyzed through equivalent circuit model fitting to provide quantitative information (Fig. 4B and fig. S13), where the impedance spectra of Li metal | separator | Li metal cells can be decoupled to interfacial resistance and bulk resistance. The interfacial resistances of Li metal cells with LLZTO ion redistributors are much lower than those of cells with routine PP separators. They remain stable at around 90 ohms in 750-hour cycling, suggesting the inhibited Li dendrites and little electrolyte consumption. However, the interface resistances exhibit large fluctuations during cycling with routine PP separators. The interfacial resistance is as large as 226.7 ohms after cycling for 1 hour and then drops to 148.5 ohms after 100-hour cycling and soars to 793.6 ohms in 750 hours. The large fluctuations indicate unstable electrochemical environments during Li depositing and striping, where Li ions are not uniformly distributed.

Post-mortem investigation of the composite separator and electrodes in the Li | Li symmetric cells before and after the cycling also confirmed the long-term stability. Sharp Li dendrites and cracks on the Li metal electrodes have been identified under the routine PP separator after cycling (fig. S14). But the surface morphologies of Li metal electrodes are comparatively smooth under the LLZTO composite separator, where only wrinkles are observed on the cycled surface. Also, the chemical compositions of the LLZTO composite separator remain unchanged after cycling (figs. S15 to S17), indicating the excellent long-term chemical stability of the ceramic coating. Morphologies of the LLZTO composite separator also demonstrate the stability during cycling. The ceramic coating with the same thickness of 5 μm is still well attached to the PP matrix without delamination (fig. S17). All these results guarantee the long-term stability of ion redistributor during repeated battery cycling.

The chemical compositions of the Li metal anodes with the addition of LLZTO ion redistributor and routine PP separators were investigated through x-ray photoelectric spectroscopy (XPS), where the components of LiF and Li_3N were detected (figs. S18 and S19 and table S2). Li_3N enables ions to transport quickly following collective a mechanism with low intracrystal migration activation energy. LiF has a large modulus in organic electrolytes, alleviating the brittle fracture of surface layer. Moreover, LiF with high surface energy to Li metal contributes to the sufficient transportations with reduced activation energy barrier to migrate Li ions. (*1*).

To demonstrate the possibility of the LLZTO composite separators in practical Li metal batteries, the electrochemical performances of LFP | Li pouch cells (Fig. 5, A and B) and Li | Li pouch cells (fig. S20) with LLZTO composite separators and routine PP separators were investigated. To ensure reproducibility, all experiments were carried out using LFP cathodes/Li metal anodes from the same roll under the same experimental conditions. Therefore, the differences in cycling performances are ascribed to the influence of separators with or without LLZTO ion redistributor facing Li metal anodes.

During cycling, the pouch cells with LLZTO composite separators exhibit higher specific capacities and excellent capacity retention compared with those of routine separators. The specific capacity of 140 mAh g^{-1} is reached at 0.1 C (1.0 C = 170 mA g^{-1}) for pouch cells with LLZTO, which maintains excellent cycling performances of 88% capacity retention until the 90th cycle. A bell-shaped charge-discharge curve is observed for both cells. The cells with LLZTO ion redistributors render the smaller polarization in the 5th and 50th cycles (40 mV), which can be attributed to the reduced dendrite formation and reduced electrolyte consumption. Symmetric Li-Li pouch cells also demonstrate the enhancement in long-term cycling stability (fig. S20). Although the cells with or without LLZTO

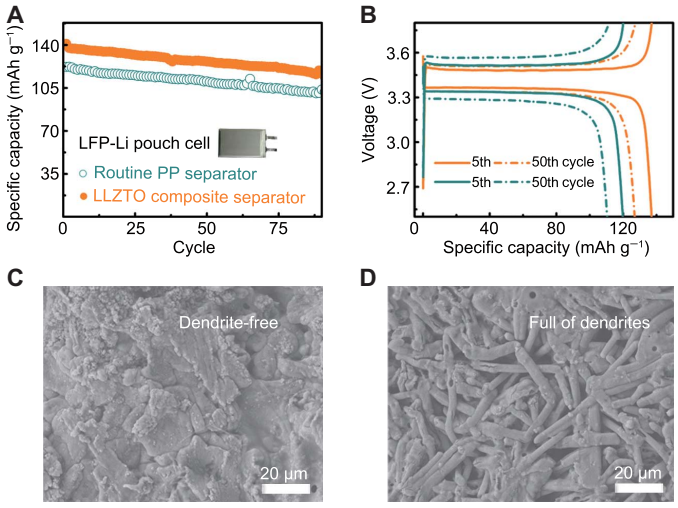

Fig. 5. Practical pouch-cell performances of LLZTO composite separators and routine PP separators. (**A**) Capacity retention with cycle numbers of pouch cells at 0.1 C. (**B**) Charge and discharge voltage profiles at the 10th cycle (solid line) and the 50th cycle (dashed line) with LLZTO a composite separator (orange) and routine PP separator (cyan). (**C** and **D**) Morphology of Li metal anodes after 90 cycles with (C) composite separators using the LLZTO layer as an ion redistributor and (D) the routine PP separator.

layers exhibit similar voltage profiles during the first cycling, the voltage of routine pouch cells (cyan line) starts to diverge at around 700 hours, indicating the Li dendrite growth and the consumption of electrolytes. Moreover, a longer life span can be expected for pouch cells with larger capacity after further optimizations such as using liquid electrolyte additives and modifying LLZTO layer thickness.

It is known that the morphology of Li metal anodes is of vital importance during cycling. Hence, ex situ SEM observations of Li anodes in LFP-Li cells were conducted after 90 cycles. A dense Li metal layer is maintained during cycling in the cells with LLZTO ion redistributors (Fig. 5C). On the contrary, sharp dendrites are observed beneath the routine PP separator accompanying the decreased specific capacity (Fig. 5D). Previous studies revealed that larger total surface areas resulted in more electrolyte consumptions. Hence, inhibiting Li dendrites through a LLZTO ion redistributor contributes to the stable cycling stability and prolonged cycle life, which is consistent with the electrochemical performances. Therefore, using composite separators with LLZTO ion redistributors enables the advanced cell design for advanced Li metal batteries with high energy density.

DISCUSSIONS

We have developed the LLZTO film as an ion redistributor and achieved a dendrite-free Li metal anode with enhanced cycling performances. Some features for the ion redistributors are required for uniform metal deposition.

First, providing the abundant ion conducting channels at working temperatures is necessary to redistribute ions effectively. To prove the concept, polyacrylonitrile (PAN) film with a similar thickness of 5 μm was used for Li metal electrodes in Li | Li symmetrical cells (fig. S21), whose ionic conductivity is lower compared with that of LLZTO at room temperature (*22*). The extended voltage hysteresis exhibits much larger overpotential to conduct Li ions, and the transport resistances increase during cycling, indicating the failure in constructing an effective ion transportation pathway with high ionic conductivity (fig. S21C).

Furthermore, the sufficient ionic conduction of a solid electrolyte layer is essential despite the fact that liquid electrolytes can infiltrate the layer, especially during long-time cycling. To figure out whether the Li ionic conductor coating is essential for Li metal batteries, we used the composite separator with a PP matrix and aluminum oxide (Al_2O_3) film, where Al_2O_3 itself cannot conduct Li ions and liquid electrolyte (or swelled polymer) is almost the only channel for Li migration. The Al_2O_3 composite separator has the same PP matrix and an aluminum oxide ceramic coating presenting a similar thickness to a LLZTO composite separator following the same preparation process (fig. S22).

To compare the electrochemical performances, symmetrical Li metal | separator | Li metal cells based on both carbonate-based (fig. S23) and ether-based (fig. S24) electrolytes cycling at a high current density of 1.0 mA cm^{-2} were investigated, where the same amounts of 7.0 μl cm^{-2} electrolyte were added. For EC/DEC electrolytes, the voltage hysteresis of Li | Li cells using Al_2O_3 ceramic layers (royal line) is narrow and similar to the batteries using LLZTO ion redistributors during the first 200-hour cycling, demonstrating that the liquid phase can also help migrate Li ions. However, after repeated cycling, the voltage polarization of Li | Li cells with Al_2O_3 ceramic layers diverge after 600 hours, suggesting that the electrolyte is nearly depleted. In comparison, the stable cycling performances of cells with a LLZTO composite separator indicate that the multiple ion transportation channels contribute to a uniform Li metal electrode without huge electrolyte consumptions. A similar behavior can be observed in DOL/DME electrolytes (fig. S24). The interfacial resistances measured at the end of 1-, 100-, and 750-hour cycling also demonstrate that sufficient ionic conduction in ceramic layer contributes to transport Li ions effectively during extended cycles (fig. S25). Simulations by finite element method (FEM) also reveal that 42.8% of Li-ion flux is transported through LLZTO ion conductor particles with limited liquid electrolytes, and the fraction is 12.6% with sufficient liquid electrolytes. Nonconductive ceramic particles such as Al_2O_3 will greatly reduce the capacity for ion conduction (fig. S26). Hence, an ion redistributor with sufficient ionic conductivity is of vital importance in the practical application of Li metal anodes, especially with limited liquid electrolytes during long-time cycling.

Incidentally, although high mechanical strength is thought to suppress Li dendrite growth and enhance the safety factor, the comparison between Al_2O_3 composite separator (Young's modulus of 9.60 GPa) and LLZTO composite separator (Young's modulus of 2.08 GPa) indicates that high mechanical strength itself alone cannot guarantee a stable cycling (fig. S27).

Moreover, moderate thickness is essential to redistribute ions efficiently. For instance, a much thicker LLZTO film with a thickness of 30 μm leads to the increase in voltage polarization of Li | Li cells (fig. S28), where ion migration paths are prolonged due to the increased electrolyte thickness, and the cells gain additional weight. On the other hand, the solid-state Li-ion conductors that are too puny to redistribute ions also exhibit limitations. As shown in fig. S29, the isolated LLZTO particles are unable to provide continuous Li-ion diffusion ways; thus, the voltage profiles show fluctuations during cycling, indicating an unstable Li deposition.

Therefore, an effective ion redistributor must satisfy ionic conductivity, moderate thickness, and the ability to form continuous ion diffusion paths. Accordingly, ideal choices for ion redistributors in Li batteries cover various fast ionic conductors, such as

$Li_{1+x}Al_xTi_{2-x}(PO_4)_3$, $Li_{10}GeP_2S_{12}$, and lithium phosphorus oxynitride, while more issues such as the chemical/electrochemical stability against Li metal must be addressed before application. Furthermore, the concept of using fast ionic conductors as ion redistributor layers to achieve a uniform metal deposition can also be extended in other energy storage systems, such as sodium metal batteries.

In summary, we propose a general approach of ion redistributors to even out the distribution of Li ions uniform for dendrite-free deposition by using a fast ionic conductor layer on commercial porous PP separators. In routine Li metal batteries, Li ions can only migrate through the pores of PP separators with liquid electrolytes. Therefore, Li ions are very crowded near the separator pores after crossing the separators. This leads to the enrichment of Li ions on the anode surface facing the pores of the separators, while there is a lack of Li ions on the anode surface facing the skeletons of the separators. The emerging composite separator consists of a LLZTO layer and a commercial PP separator as a matrix. The LLZTO layer works as an ion redistributor to release the congestion of ions and guide Li ions to deposit uniformly. Beneath the LLZTO composite separator, the SD of ion concentration is 13 times less than that beneath the routine PP separator. The Coulombic efficiencies of Li metal anodes in Li | Cu cells are above 98% over 450 cycles. The polarization of Li metal electrodes are limited to 80 mV, with ion redistributors at a high current density of 1.0 mA cm^{-2} for 800 hours. These composite separators alleviate Li dendrite formation, contributing to the reduced electrolyte consumption and enabling the very little liquid that electrolytes use for Li anodes. Therefore, the battery's safety is greatly enhanced. The improvement of cells with LLZTO ion redistributors is proved through the simulation of Li-ion migration, Li depositing morphology, and long-term cycling performance. An LFP | Li metal pouch cell renders an excellent specific capacity of above 140 mAh g^{-1} and maintains 88% capacity retention until the 90th cycle, demonstrating the feasibility of using solid-state Li ionic conductors as ion redistributors in practical Li metal batteries. This facile but effective approach can also be extended to various battery systems such as sodium batteries by substituting LLZTO with other fast ionic conductors.

MATERIALS AND METHODS

Preparation of composite separators

The routine PP separators used were Celgard 2400. The Al-doped $Li_{6.75}La_3Zr_{1.75}Ta_{0.25}O_{12}$ (LLZTO) powders were purchased from WuXi Kai-Star Electro-Optic Materials Co. Ltd and ball milled before use. First, LLZTO powders were dispersed in THF solvent with a concentration of around 5.0 mg ml^{-1}. The suspension was sonicated for 4 hours and centrifuged at 500 rpm for 10 min to remove bulk powders. Then, a polyvinylidene fluoride (PVDF) binder was added with the mass ratio of LLZTO and PVDF at 9:1. The LLZTO powders and PVDF binder in THF suspension were coated on one side of the Celgard 2400 separator through vacuum filtration. The composite separators for pouch cells were synthesized by doctor blading after adjusting the viscosity of the suspension. The composite separator was dried at room temperature overnight.

Materials characterization

The morphology of the composite separator was characterized on a JEOL JSM-7401F SEM operated at 3.0 kV and a JEM-2010 TEM operated at 120.0 kV. The crystallographic structure was examined by XRD (Bruker D8 Advance) with Cu Kα radiation and 2θ in the range of 5° to 90° at 2.5° min^{-1}. The XPS analysis was carried out with Al Kα radiation (72 W, 12 kV) at a pressure of 10^{-9} torr and an argon ion beam. Thermogravimetric analysis (TGA) tests were carried out from 30° to 900°C (TA Instruments, Q5000IR).

Electrochemical cycling tests

LFP cathodes were synthesized from 80% LFP powders (MTI Kejing Group), 10% super P carbon blacks, and 10% PVDF binder. The three components were fully mixed in *N*-methyl-2-pyrrolidone (Peking Reagent Modern Oriental Technology Development), and the resultant slurry was coated on aluminum foil using a doctor blade. The electrodes were dried for 48 hours before use. The LFP cathode foil was punched for a 60 mm by 40 mm pouch cell. The typical active material loading was about 5.0 mg cm^{-2}. Commercial Li metal foils with the thickness of 50 μm were purchased from China Energy Lithium Co. Ltd.

The carbonate-based electrolytes were 1.0 M $LiPF_6$ dissolved in EC/DEC (1:1 in volume) without other additives. The ether-based electrolytes were 1.0 M Li bis(trifluoromethane-sulfonyl)imide DOL/DME. The electrolytes used in Li | Cu cells in Fig. 4A were DOL/DME with 5.0 weight % lithium nitrate ($LiNO_3$), while other ether-based electrolytes were used without any additives. The liquid electrolytes used in all batteries were 7.0 μl cm^{-2}. Li | Li symmetric coin cells and Li | Cu cells were assembled with 2032 coin-type cells. Lithium was plated and stripped for 2 hour per cycle in Li | Li cells and for 2 hours per cycle in Li | Cu cells. In Li | Cu cells, the capacity of 0.5 mAh cm^{-2} Li was deposited on bare copper substrate and set to be totally stripped in one cycle. All batteries were assembled in an Ar-filled glove box with O_2 and H_2O content below 0.5 parts per million. The interfacial resistance was tested via electrochemical impedance spectroscopy measurement (0.1×10^6 Hz) with a Solartron 1470E electrochemical workstation. The LFP pouch cells were cycled in a galvanostatic mode with a voltage range of 2.5 to 3.8 V.

Simulations of Li-ion distribution through separators

FEM conducted by COMSOL Multiphysics was used to investigate the distribution of Li ions through a routine PP separator and LLZTO composite separator. The migration of Li ions driven by electric field and diffusion flow in both liquid phase (electrolytes) and solid phase (LLZTO particles) was taken into account in these simplified simulations. Two physical models of electrostatic and transport of diluted species based on the partial differential equations listed below were coupled to conduct FEM simulation.

$$\mathbf{E} = -\nabla\varphi \tag{1}$$

$$\mathbf{N} = -D\nabla c + \mu c\mathbf{E} \tag{2}$$

$$\frac{\partial c}{\partial t} = -\nabla\mathbf{N} \tag{3}$$

where φ is the electric potential, **E** is the electric field, *D* is the diffusion coefficient of Li ion, *c* is the concentration of Li ion, μ is the ionic mobility of Li ion in electrolytes, and **N** is the flux vector of Li ion. These FEM simulations on the routine PP separator and the LLZTO composite separator were performed in a rectangle area with a size of 30.0 μm by 45.0 μm and 30.0 μm by 50.0 μm, respectively. The routine PP separator was simplified as a sieve plate with a thickness of 25.0 μm, which consists of narrow rectangular channels with a pore size of 1.0 μm

and a pore spacing of 1.0 μm (fig. S5). The LLZTO composite separator was simplified as a two-layered sieve plate. The upper layer is the same as the routine PP separator. The under layer with a thickness of 5.0 μm consists of 14 rows of close-packed spherical particles with a particle size of 0.36 μm and a gap of 0.04 μm, which is representing the LLZTO layer (fig. S5). It should be noticed that the sizes in these simulations are representative selected on the basis of the feasibility of FEM modeling and physical sizes according to SEM images (Fig. 2, B and C) and the size distribution of LLZTO. However, this model cannot fully reflect the real circumstance; it can only offer valuable fundamental understandings in ideal systems, since the practical pore structure and pore size distribution are much more complex. In addition, to compare the Li ion distribution near the anode electrode surface after the two transportation behaviors of Li ions through routine PP separator and LLZTO composite separator, the spacing between the electrode and the separator is set to the same distance of 10.0 μm. The potential difference $\Delta\varphi$ through these electrolytes is set as 0.02 V. The diffusion coefficients D of Li ions in liquid electrolyte and solid LLZTO particles are set as 3.0×10^{-10} m^2 s^{-1} and 6.0×10^{-12} m^2 s^{-1}, respectively. To investigate the ion transport behaviors with limited liquid electrolytes in long-time cycling, the same physical model was established and the ratio of diffusion coefficients of Li ions in liquid electrolytes and solid LLZTO particles was decreased to 10.0. The mobilities of Li ions μ for liquid electrolyte and solid LLZTO particles are defined by the Nernst-Einstein equation. The bottom boundaries of two simulation areas are the Dirichlet boundaries with $\varphi_0 = 0$ V and $c_0 = 0$ M. The top boundaries of two simulation area are also Dirichlet boundaries with $\varphi_1 = 0.02$ V and $c_1 = 1.0$ M (fig. S5). The other boundaries are natural boundaries with zero flux.

SUPPLEMENTARY MATERIALS

Supplementary material for this article is available at http://advances.sciencemag.org/cgi/content/full/4/11/eaat3446/DC1

Fig. S1. XRD patterns of the LLZTO composite separator (orange), LLZTO powder (cyan), and the powder diffraction file (PDF) of $Li_5La_2Nb_2O_{12}$.
Fig. S2. TEM images of the LLZTO ceramic powders.
Fig. S3. SEM image for the surface of commercial PP separator (Celgard 2400).
Fig. S4. TGA curves of routine PP separator (cyan) and LLZTO composite separator (orange) in nitrogen or oxygen atmosphere.
Fig. S5. FEM models for the routine PP separator (without LLZTO layer) and the composite separator (with LLZTO layer).
Fig. S6. The relative concentration of Li ions beneath the routine PP separator (cyan line) and the composite separator (orange line) at $y = 9.0$ μm in the FEM simulation results (Fig. 3, A and B).
Fig. S7. Schematic illustration of the electrolytic cells designed for electrochemical deposition to avoid the effect of stress.
Fig. S8. Schematic illustration of the coin cells designed for electrochemical deposition to avoid the effect of stress and maintain the close contact between LLZTO ion redistributors and electrodes.
Fig. S9. SEM images of Li metal deposits in coin cells with PTFE circle.
Fig. S10. Charge and discharge voltage profiles of Li | Cu cells.
Fig. S11. Voltage profiles for Li | Li symmetric cells using carbonate-based EC/DEC electrolytes at a current density of 0.5 mA cm^{-2}.
Fig. S12. Voltage profiles for Li | Li symmetric cells using ether-based DOL/DME electrolytes at a current density of 0.5 mA cm^{-2}.
Fig. S13. Impedance spectra of Li | Li cells.
Fig. S14. SEM images of Li metal electrodes in Li | Li symmetric cells.
Fig. S15. XPS survey of LLZTO layer on composite separators.
Fig. S16. XPS spectra of LLZTO layer on composite separators.
Fig. S17. Morphological characterizations of the LLZTO composite separator after cycling.
Fig. S18. XPS spectra of the deposited Li metal anode surface with the LLZTO composite separator in DOL/DME electrolytes.
Fig. S19. XPS spectra of the deposited Li metal anode surface with the routine PP separator in DOL/DME electrolytes.
Fig. S20. Voltage hysteresis of Li | Li pouch cells with EC/DEC electrolytes at a current density of 0.25 mA cm^{-2}.
Fig. S21. Morphology and cycling performances of the separator with PAN layer of lower ionic conductivity compared with the LLZTO composite separator of the LLZTO film.
Fig. S22. Morphology of the composite separator with Al_2O_3 layer.
Fig. S23. Cycling performances of the composite separator with Al_2O_3 and LLZTO coating layer.
Fig. S24. Cycling performances of the composite separator with Al_2O_3 layer and LLZTO coating layers.
Fig. S25. Electrochemical impedances of Li | Li symmetrical cells in EC/DEC electrolytes at 1.0 mA cm^{-2}.
Fig. S26. Ion transportation behaviors in the composite separator with a LLZTO ion conductive layer and a Li-ion insulator layer when limited liquid electrolytes are adopted.
Fig. S27. Atomic force microscopy analysis of the LLZTO composite separator and the Al_2O_3 composite separator.
Fig. S28. Morphology and cycling performances of the separator with a thicker LLZTO film (30 μm) to redistribute Li ions compared with the LLZTO composite separator of the 5-μm LLZTO film.
Fig. S29. Morphology and cycling performances of the separator with isolated LLZTO particles compared with the LLZTO composite separator of the 5-μm LLZTO film.
Table S1. Statistics of the concentration of Li ions beneath the routine PP separator and the composite separator at $y = 9.0$ μm.
Table S2. Element atomic percentage of Li metal anode surface with the LLZTO composite separator and the routine PP separator obtained from XPS spectra.

REFERENCES AND NOTES

1. Z. Tu, P. Nath, Y. Lu, M. D. Tikekar, L. A. Archer, Nanostructured electrolytes for stable lithium electrodeposition in secondary batteries. *Acc. Chem. Res.* **48**, 2947–2956 (2015).
2. M. D. Tikekar, L. A. Archer, D. L. Koch, Stabilizing electrodeposition in elastic solid electrolytes containing immobilized anions. *Sci. Adv.* **2**, e1600320 (2016).
3. M. D. Tikekar, S. Choudhury, Z. Tu, L. A. Archer, Design principles for electrolytes and interfaces for stable lithium-metal batteries. *Nat. Energy* **1**, 16114 (2016).
4. M. R. Busche, T. Drossel, T. Leichtweiss, D. A. Weber, M. Falk, M. Schneider, M.-L. Reich, H. Sommer, P. Adelhelm, J. Janek, Dynamic formation of a solid–liquid electrolyte interphase and its consequences for hybrid-battery concepts. *Nat. Chem.* **8**, 426–434 (2016).
5. S. Choudhury, C. T.-C. Wan, W. I. Al Sadat, Z. Tu, S. Lau, M. J. Zachman, L. F. Kourkoutis, L. A. Archer, Designer interphases for the lithium-oxygen electrochemical cell. *Sci. Adv.* **3**, e1602809 (2017).
6. Q. Pang, X. Liang, A. Shyamsunder, L. F. Nazar, An in vivo formed solid electrolyte surface layer enables stable plating of Li metal. *Joule* **1**, 871–886 (2017).
7. A. Wang, S. Tang, D. Kong, S. Liu, K. Chiou, L. Zhi, J. Huang, Y.-Y. Xia, J. Luo, Bending-tolerant anodes for lithium-metal batteries. *Adv. Mater.* **30**, 1703891 (2018).
8. C.-P. Yang, Y.-X. Yin, S.-F. Zhang, N.-W. Li, Y.-G. Guo, Accommodating lithium into 3D current collectors with a submicron skeleton towards long-life lithium metal anodes. *Nat. Commun.* **6**, 8058 (2015).
9. C. Zu, A. Manthiram, Stabilized lithium–metal surface in a polysulfide-rich environment of lithium–sulfur batteries. *J. Phys. Chem. Lett.* **5**, 2522–2527 (2014).
10. E. Markevich, G. Salitra, D. Aurbach, Fluoroethylene carbonate as an important component for the formation of an effective solid electrolyte interphase on anodes and cathodes for advanced Li-ion batteries. *ACS Energy Lett.* **2**, 1337–1345 (2017).
11. J.-K. Kim, D. H. Kim, S. H. Joo, B. Choi, A. Cha, K. M. Kim, T.-H. Kwon, S. K. Kwak, S. J. Kang, J. Jin, Hierarchical chitin fibers with aligned nanofibrillar architectures: A nonwoven-mat separator for lithium metal batteries. *ACS Nano* **11**, 6114–6121 (2017).
12. J. Zhi, A. Z. Yazdi, G. Valappil, J. Haime, P. Chen, Artificial solid electrolyte interphase for aqueous lithium energy storage systems. *Sci. Adv.* **3**, e1701010 (2017).
13. H. Duan, Y.-X. Yin, Y. Shi, P. F. Wang, X.-D. Zhang, C.-P. Yang, J.-L. Shi, R. Wen, Y.-G. Guo, L.-J. Wan, Dendrite-free Li-metal battery enabled by a thin asymmetric solid electrolyte with engineered layers. *J. Am. Chem. Soc.* **140**, 82–85 (2018).
14. J. Li, C. Ma, M. Chi, C. Liang, N. J. Dudney, Solid electrolyte: The key for high-voltage lithium batteries. *Adv. Energy Mater.* **5**, 1401408 (2015).
15. J. Zhang, J. Zhao, L. Yue, Q. Wang, J. Chai, Z. Liu, X. Zhou, H. Li, Y. Guo, G. Cui, L. Chen, Safety-reinforced poly(propylene carbonate)-based all-solid-state polymer electrolyte for ambient-temperature solid polymer lithium batteries. *Adv. Energy Mater.* **5**, 1501082 (2015).
16. D. Zhou, R. Liu, J. Zhang, X. Qi, Y.-B. He, B. Li, Q.-H. Yang, Y.-S. Hu, F. Kang, In situ synthesis of hierarchical poly(ionic liquid)-based solid electrolytes for high-safety lithium-ion and sodium-ion batteries. *Nano Energy* **33**, 45–54 (2017).
17. T. Liu, Z. Chang, Y. Yin, K. Chen, Y. Zhang, X. Zhang, The PVDF-HFP gel polymer electrolyte for Li-O_2 battery. *Solid State Ion.* **318**, 88–94 (2018).
18. J. L. Schaefer, Y. Lu, S. S. Moganty, P. Agarwal, N. Jayaprakash, L. A. Archer, Electrolytes for high-energy lithium batteries. *Appl. Nanosci.* **2**, 91–109 (2011).
19. S. Choudhury, Z. Tu, S. Stalin, D. Vu, K. Fawole, D. Gunceler, R. Sundararaman, L. A. Archer, Electroless formation of hybrid lithium anodes for fast interfacial ion transport. *Angew. Chem. Int. Ed.* **56**, 13070–13077 (2017).

20. N. B. Aetukuri, S. Kitajima, E. Jung, L. E. Thompson, K. Virwani, M.-L. Reich, M. Kunze, M. Schneider, W. Schmidbauer, W. W. Wilcke, D. S. Bethune, J. C. Scott, R. D. Miller, H.-C. Kim, Flexible ion-conducting composite membranes for lithium batteries. *Adv. Energy Mater.* **5**, 1500265 (2015).
21. L. Fan, H. L. Zhuang, L. Gao, Y. Lu, L. A. Archer, Regulating Li deposition at artificial solid electrolyte interphases. *J. Mater. Chem. A* **5**, 3483–3492 (2017).
22. A. Manthiram, X. Yu, S. Wang, Lithium battery chemistries enabled by solid-state electrolytes. *Nat. Rev. Mater.* **2**, 16103 (2017).
23. J. C. Bachman, S. Muy, A. Grimaud, H.-H. Chang, N. Pour, S. F. Lux, O. Paschos, F. Maglia, S. Lupart, P. Lamp, L. Giordano, Y. Shao-Horn, Inorganic solid-state electrolytes for lithium batteries: Mechanisms and properties governing ion conduction. *Chem. Rev.* **116**, 140–162 (2016).
24. N.-W. Li, Y. Shi, Y.-X. Yin, X.-X. Zeng, J.-Y. Li, C.-J. Li, L.-J. Wan, R. Wen, Y.-G. Guo, A flexible solid electrolyte interphase layer for long-life lithium metal anodes. *Angew. Chem. Int. Ed.* **57**, 1505–1509 (2017).
25. Y. Li, B. Xu, H. Xu, H. Duan, X. Lü, S. Xin, W. Zhou, L. Xue, G. Fu, A. Manthiram, J. B. Goodenough, Hybrid polymer/garnet electrolyte with a small interfacial resistance for lithium-ion batteries. *Angew. Chem. Int. Ed.* **56**, 753–756 (2017).
26. W. Luo, L. Zhou, K. Fu, Z. Yang, J. Wan, M. Manno, Y. Yao, H. Zhu, B. Yang, L. Hu, A thermally conductive separator for stable Li metal anodes. *Nano Lett.* **15**, 6149–6154 (2015).
27. H. Lee, X. Ren, C. Niu, L. Yu, M. H. Engelhard, I. Cho, M.-H. Ryou, H. S. Jin, H.-T. Kim, J. Liu, W. Xu, J.-G. Zhang, Suppressing lithium dendrite growth by metallic coating on a separator. *Adv. Funct. Mater.* **27**, 1704391 (2017).
28. J.-Y. Wu, S.-G. Ling, Q. Yang, H. Li, X.-X. Xu, L.-Q. Chen, Forming solid electrolyte interphase in situ in an ionic conducting $Li_{1.5}Al_{0.5}Ge_{1.5}(PO_4)_3$-polypropylene (PP) basedseparator for Li-ion batteries. *Chin. Phys. B* **25**, 78204 (2016).
29. F. Han, Y. Zhu, X. He, Y. Mo, C. Wang, Electrochemical stability of $Li_{10}GeP_2S_{12}$ and $Li_7La_3Zr_2O_{12}$ solid electrolytes. *Adv. Energy Mater.* **6**, 1501590 (2016).
30. J. L. Allen, J. Wolfenstine, E. Rangasamy, J. Sakamoto, Effect of substitution (Ta, Al, Ga) on the conductivity of $Li_7La_3Zr_2O_{12}$. *J. Power Sources* **206**, 315–319 (2012).
31. W. G. Zeier, Structural limitations for optimizing garnet-type solid electrolytes: A perspective. *Dalton Trans.* **43**, 16133–16138 (2014).
32. E. J. Cussen, Structure and ionic conductivity in lithium garnets. *J. Mater. Chem.* **20**, 5167–5173 (2010).
33. L. J. Miara, S. P. Ong, Y. Mo, W. D. Richards, Y. Park, J.-M. Lee, H. S. Lee, G. Ceder, Effect of Rb and Ta doping on the ionic conductivity and stability of the garnet $Li_{7+2x-y}(La_{3-x}Rb_x)(Zr_{2-y}Ta_y)O_{12}$ ($0 \leq x \leq 0.375$, $0 \leq y \leq 1$) superionic conductor: A first principles investigation. *Chem. Mater.* **25**, 3048–3055 (2013).
34. M. Xu, M. S. Park, J. M. Lee, T. Y. Kim, Y. S. Park, E. Ma, Mechanisms of Li^+ transport in garnet-type cubic $Li_{3+x}La_3M_2O_{12}$(M= Te, Nb, Zr). *Phys. Rev. B* **85**, 052301 (2012).
35. C. A. Geiger, E. Alekseev, B. Lazic, M. Fisch, T. Armbruster, R. Langner, M. Fechtelkord, N. Kim, T. Pettke, W. Weppner, Crystal chemistry and stability of "$Li_7La_3Zr_2O_{12}$" garnet: A fast lithium-ion conductor. *Inorg. Chem.* **50**, 1089–1097 (2011).
36. V. Thangadurai, S. Narayanan, D. Pinzaru, Garnet-type solid-state fast Li ion conductors for Li batteries: Critical review. *Chem. Soc. Rev.* **43**, 4714–4727 (2014).
37. A. Logéat, T. Köhler, U. Eisele, B. Stiaszny, A. Harzer, M. Tovar, A. Senyshyn, H. Ehrenberg, B. Kozinsky, From order to disorder: The structure of lithium-conducting garnets $Li_{7-x}La_3Ta_xZr_{2-x}O_{12}$ (x = 0–2). *Solid State Ion.* **206**, 33–38 (2012).
38. R. Chen, W. Qu, X. Guo, L. Li, F. Wu, The pursuit of solid-state electrolytes for lithium batteries: From comprehensive insight to emerging horizons. *Mater. Horiz.* **3**, 487–516 (2016).
39. J. Zheng, M. Tang, Y.-Y. Hu, Lithium ion pathway within $Li_7La_3Zr_2O_{12}$-polyethylene oxide composite electrolytes. *Angew. Chem. Int. Ed.* **55**, 12538–12542 (2016).
40. B. D. Adams, J. Zheng, X. Ren, W. Xu, J.-G. Zhang, Accurate determination of Coulombic efficiency for lithium metal anodes and lithium metal batteries. *Adv. Energy Mater.* **8**, 1702097 (2017).

Acknowledgments: We acknowledge the support from Tsinghua National Laboratory for Information Science and Technology for theoretical simulations. We thank J. Dong, R. Xu, and H.-J. Peng for discussion. **Funding:** This work was supported by the National Key Research and Development Program (2016YFA0202500, 2016YFA0200102, and 2015CB932500), the National Natural Science Foundation of China (21676160, 21805161, and 21808121), the China Postdoctoral Science Foundation (2018M631480 and BX201700125), the Tsinghua National Laboratory for Information Science and Technology, and the Tsinghua University Initiative Scientific Research Program. **Author contributions:** Q.Z. and X.-B.C. conceived the idea. C.-Z.Z. carried out the synthesis of ion redistributors for batteries, C.-Z.Z. and P.-Y.C. conducted the electrochemical evaluation. R.Z. and X.C. conducted theoretical modeling and simulation. B.-Q.L. conducted TEM characterization. X.-Q.Z. conducted full cell batteries. Q.Z. supervised the project. C.-Z.Z., X.-B.C., and Q.Z. wrote the manuscript. All authors discussed the results and commented on the manuscript. **Competing interests:** The authors declare that they have no competing interests. **Data and materials availability:** All data needed to evaluate the conclusions in the paper are present in the paper and/or the Supplementary Materials. Additional data related to this paper may be requested from the authors.

Submitted 16 February 2018
Accepted 4 October 2018
Published 9 November 2018
10.1126/sciadv.aat3446

Citation: C.-Z. Zhao, P.-Y. Chen, R. Zhang, X. Chen, B.-Q. Li, X.-Q. Zhang, X.-B. Cheng, Q. Zhang, An ion redistributor for dendrite-free lithium metal anodes. *Sci. Adv.* **4**, eaat3446 (2018).